Characterization of A Novel Open-Ended Shock Tube Facility Based on Detonation Transmission Tubing

Guoshuai Li[a*], Takahiro Ukai[b], Konstantinos Kontis[a]

[a]*University of Glasgow, School of Engineering, Glasgow, G12 8QQ, UK*

[b]*Osaka Institute of Technology, Osaka, 535-8585, Japan*

[*]**Corresponding author:** ***GUOSHUAI LI***

email: *g.li.1@research.gla.ac.uk*

Telephone: + 44-7423309223

Abstract:

This paper proposes and demonstrates a novel shock tube driven by commercially available detonation transmission tubing in a safe, repeatable, and controllable manner for laboratory scale experiments. A circular cross-sectional open-ended shock tube (inner-diameter D = 22 mm) driven by detonation transmission tubing was used to investigate the working principle of this novel shock tube using a dynamic pressure transducer and time-resolved shadowgraph photography. Specifically, the shock Mach number, repeatability, and flow structure generated from the tube exit were characterized. The experimental result shows that the flow structure including an initial shock wave, a vortex ring, an embedded shock, and an oblique shock pattern is similar to that of the conventional compressed-gas driven shock tubes. Furthermore, the shock tube has good repeatability of less than 2% with a shock Mach number up to 1.58. The versatile and cost-effective nature of the shock tube driven by detonation transmission tubing opens a new horizon for shock wave-assisted interdisciplinary applications.

Keywords: Shock tube, Detonation transmission tubing, Flow structure, Repeatability, Shock Mach number

1. Introduction

Shock tubes are an exceptional valuable facility that can produce both high pressure and high temperature jump during a short period [1-3]. A typical shock tube consists of two sections: the driver and driven sections. A high pressure gas in the driver section is separated by a diaphragm from the driven section filled in relatively lower pressure gas. Once the diaphragm ruptures, the driver gas expands into the driven section, thereby propagating a shock wave and an expansion wave to the driven and driver tubes, respectively. The shock wave produces a high pressure and a high temperature as well as induced high speed flow. Since the magnitude of these flow features depends on the initial pressure ratio between the driver and driven sections as well as the specific heat ratio of gas medium, shock tubes can be used to study aerodynamic flows in a wide range of temperatures and pressures, which are difficult to obtain in other types of testing facilities [4-16]. Additionally, shock tubes are applicable to fundamental research in medicine, biology, and industries [17-23].

The conventional shock tubes are generally large in size and have a high cost of conducting tests and maintenance because more money should be spent on construction and maintenance of the high pressure gas system and the diaprhragm. In recent years, there has been substantial progress regarding shock tubes less expensive and easier to operate. Downey, *et al.* [24] designed a diaphragmless shock tube facility using a rapid opening valve which is the same as the function of a bursting diaphragm. The opening time of the rapid valve was on a timescale of 0.5 ms. Taylor [25] proposed a similar diaphragmless design concept, employing a shock wave generating mechanism that consists of a rotating door and a locking cam-shaft system. Furthermore, Janardhanraj and Jagadeesh [26] presented a novel concept to generate miniature shock waves using an in-situ oxyhydrogen generator. The shock tube operated in a forward-facing detonation driver mode and there was no need for storage of high pressure gases. The required amount of oxyhydrogen mixture was generated using alkaline electrolysis that produced hydrogen and oxygen gases in stoichiometric quantity. Kai *et al.* [27] demonstrated a novel method to generate shock waves in small tubes. In their design, a femtosecond laser was applied to generate an optical breakdown of an aluminium film as target. Due to the rapid appearance of this non-equilibrium state of the target, a shock wave was induced.

The present study proposes and demonstrates a novel concept to design the shock tube using a commercially available and cost-effective detonation transmission tubing. The detonation transmission tubing had been applied to generate micro-blast waves or small-scale explosion in previous studies [12, 28, 29]. Additionally, Ukai *et al.* [12] used the shock tube driven by a high pressure explosion gas produced from the detonation transmission tubing for the first time to investigate shock wave distortion in shock-square vortex loop interaction. However, the working principle of the detonation transmission

tubing driven shock tube and capabilities of this type of the shock tube have not been investigated yet. In this study, a circular cross-sectional open-ended shock tube driven by the detonation transmission tubing was employed. To investigate the flow features and capabilities of the shock tube, the pressure measurement in the driven tube and the flow visualization were conducted. For the flow visualization images, an in-house developed software [30] based on MATLAB GUI and digital image processing techniques was used for the shock wave detection and tracking.

2. Design details

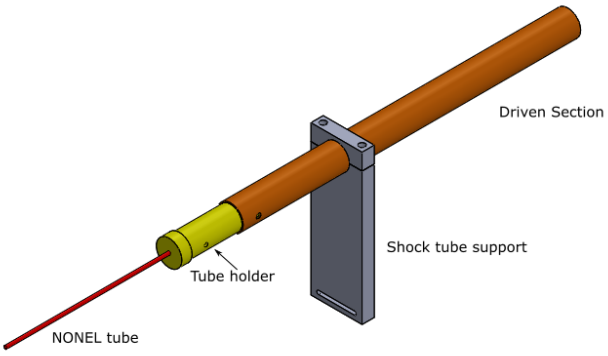

Fig 1. The shock tube by detonation transmission tubing

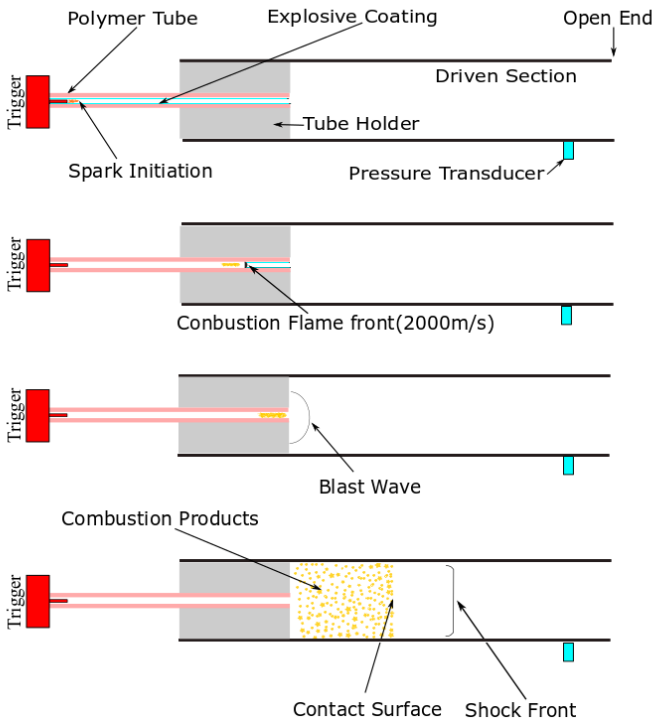

Fig 2. The working principle of the shock tube driven by detonation transmission tubing

Figures 1 and 2 present a circular cross-sectional open-ended shock tube driven by the detonation transmission tubing (inner-diameter D = 22 mm, driven section length L_d = 330 mm) and the working

principle of the shock tube, respectively. Unlike conventional compressed-gas driven shock tubes, the proposed shock tube is driven by detonation transmission tubing and there is no need for storage of high pressure gas for shock wave generation. Detonation transmission tubing, also known as NONEL tube (Dyno Nobel), is a detonation driver generally used for demolition of buildings and the rock blasting in mines and quarries. The NONEL tube is an annular small plastic tube (inner diameter: *ID* = 1.3 mm, outer diameter: *OD* = 3 mm) coated on the innermost wall with a reactive explosive compound. When the reactive explosive compound is ignited the explosive reaction travels at approximately 2,000 m/s within the tube [29]. The explosive mixture, about 18 mg/m, is predominantly HMX: High-melting explosive (~92 % by weight), along with trace of aluminium (~8% by weight). The detonation is initiated by an electronic blasting machine (Dyno Nobel, model: DynoStart 2), with an output voltage of 2500 V. As shown in Fig. 2, when the micro explosives are electrically triggered from one end of the polymer tube, the rapid expulsion of combustion gases within it causes high temperature and high pressure, which results in the same features as compressed gases in the conventional shock tube. The combustion gas compresses the ambient air and eventually leading to the formation of a hemispherical blast wave in the driven section. When the blast wave impinges on the wall of the driven section, pressure behind the blast wave becomes gradually uniform. Finally, the hemispherical shock front of the blast wave transforms to plane shape, except for a small deflection in the vicinity of the inner wall surface. Alike the compressed-gas driven shock tubes, the shock wave causes the temperature, pressure and density jumps, and these flow features are separated by a contact surface of the driver combustion gas.

To align the central axis of the flexible NONEL tube with that of the driven tube, the NONEL tube was inserted into a stainless steel tube holder (*ID* = 3 mm, *OD* = 22 mm, length L_h = 140 mm), installing into the circular cross-sectional driven tube (*ID* = 22 mm, *OD* = 25 mm). The NONEL tube was stably fixed to the tube holder using a screw on the side wall. Two through holes were manufactured at two sides of the leading edge of the driven section to install the NONEL tube holder. Additionally, two pairs of blind thread holes were manufactured at the sides of the NONEL tube holder with a 50 mm interval, which allowed the variation of the driven tube length: namely, L_d = 230 and 330 mm.

3. Experimental setup

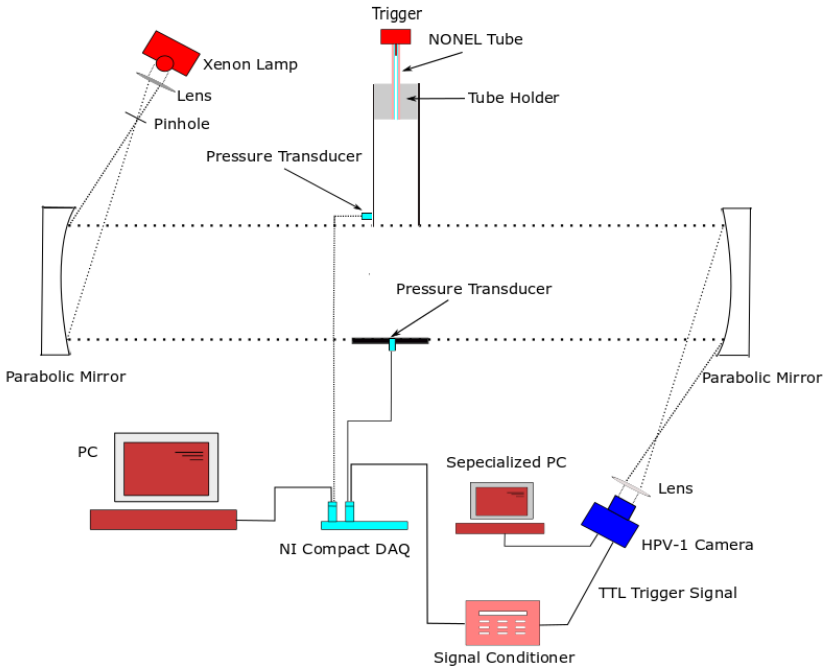

Fig 3. Schematic of the experimental setup

To investigate capabilities of the detonation transmission tubing driven open-ended shock tube, pressure measurement was performed to get the shock Mach number *Ms* from the overpressure magnitude in the driven section of the shock tube. Meanwhile, the flow structure from the open end was visualized using the time-resolved shadowgraph photography with a typical Z-type optical arrangement. A schematic diagram of the experimental setup is shown in Fig. 3. A pressure transducer (Kulite Semiconductor Products, Inc., model: XTE-190M, natural frequency: 175 kHz) was placed at 50 mm from the open end to measure the pressure history in the driven section. The pressure signal was recorded using a NI-9223 module (National Instruments Corp., 1 MS/s, 16 bit, 4 channels) with a NI-9178 compact data acquisition system driven by LabVIEW. Furthermore, the sampling rate of 1 MHz is chosen in order to get high-precision results.

The shadowgraph system consists of a 450-1000W continuous light source with a Xenon arc lamp (Newport, model: 66921), a pair of 203.3 mm diameter parabolic mirror with a focal length of 1829 mm, and a high-speed camera (Shimadzu, model: HPV-1) with a recording speed up to 1M frames per second. To synchronize the high-speed camera, the pressure rising signal induced by the shock wave was employed to trigger the camera. Specifically, another same Kulite pressure transducer embedded in a rectangular plate was placed ahead of the open end to trigger the camera (Fig. 3). A signal conditioner for converting the rising voltage output of the pressure transducer into a 5V TTL signal was specially designed.

4. Results and discussions

4.1 Shock Mach number range

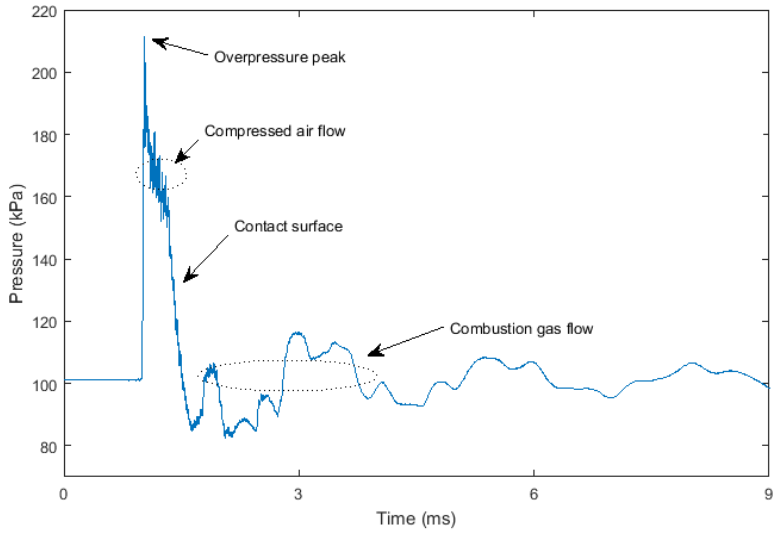

Fig. 4 Pressure-time history of the Kulite pressure transducer in the driven section (L=300mm)

Figure 4 presents the pressure history measured by the Kulite pressure transducer in the driven section. The pressure signal was filtered by a moving average (smoothing width is 14). As shown in Fig. 4, the initial pressure peak denotes the shock. When the shock wave arrives at the open end, an expansion wave is created due to shock diffraction and travels upstream. This expansion wave accelerates the out-flowing air and thereby causes the pressure to drop. This pressure drop is also shown in the conventional open-end shock tube [31]. After the contact surface passes the transducer, a sudden pressure decrease appears because of the expansion waves from the NONEL tube end and the open end of the shock tube. The expansion waves from both NONEL tube end and the open end of shock tube accelerate the out-flowing combustion gas and thereby causes its pressure to drop below the ambient pressure. Overall, the pressure profile in the driven section of the shock tube is similar to that of conventional compressed-air driven shock tubes [31]. However, the time duration of the air flow between the shock wave and the contact surface is much shorter (approximately 350 μs) than that of conventional shock tubes due to its limited dimensions (the length of the driven section is only 330 mm).

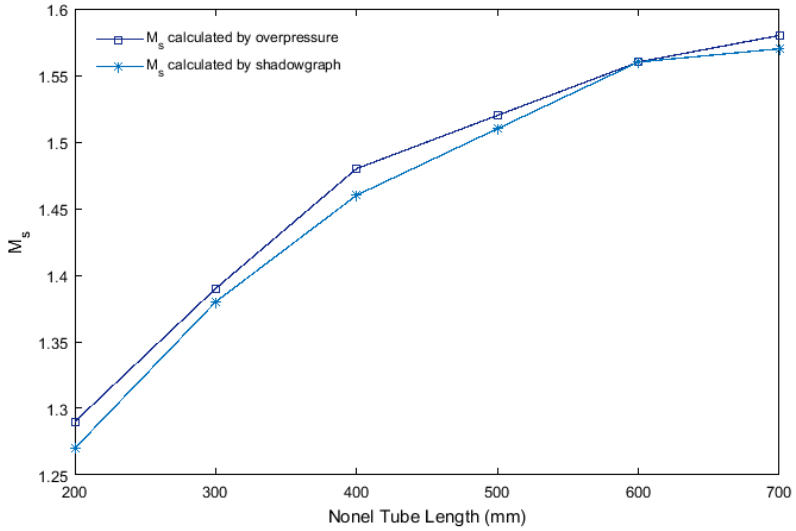

Fig. 5 Shock Mach number and overpressure in different NONEL tube lengths

Table 1 Shock wave Mach numbers M_s in different detonation transmission tubing lengths

***L* mm**	***Explosive mixture* mg**	***M_s* by peak overpressure**	***M_s* by shadowgraph**
200	3.6	1.29	1.27
300	5.4	1.39	1.38
400	7.2	1.48	1.46
500	9.0	1.52	1.51
600	10.8	1.56	1.56
700	12.6	1.58	1.57

The shock Mach number M_s can be estimated using the normal shock wave theory [26]:

$$\frac{P_s}{P_a} = 1 + \frac{2\gamma}{\gamma+1}(M_s^2 - 1) \quad (1)$$

where P_a *and* P_s denote the ambient pressure in front of the shock wave and the initial overpressure behind the shock wave, respectively. ?? = 1.4 is the specific heat ratio of the compressed gas in front of the combustion gas. The shock velocity released from the open end can be calculated by automatically detecting and tracking the initial shock wave from shadowgraph images as well. In this study, the shock velocity was calculated by detecting the shock positions of first five shadowgraph

images (4μs time interval between each image) from the open end and the calculating process was conducted using an in-house developed software [30], in which computer vision algorithms such as background subtraction in frequency domain, adaptive threshold and sub-pixel interpolation were utilized.

Figure 5 shows the shock Mach number M_s calculated both by the overpressure and shadowgraph images for NONEL tube length L = 200 to 700 mm. Additionally, more specific shock Mach number is given in Table 1. As shown in Fig. 5, M_s calculated by the overpressure basically corresponds to that of the shadowgraph images. However, M_s obtained through the overpressure is higher than that of the shadowgraph images as a whole. That makes sense because the shock wave is dissipative after it emits from the open end of the shock tube. Moreover, it is apparent that the longer NONEL tube has higher denotation energy and generates a stronger shock wave; however, the shock Mach number non-linearly increases. When the NONEL tube length is over 400 mm, the shock Mach number increases very slightly. Specifically, the shock Mach number range of this novel shock tube is around from 1.29 to 1.58 (NONEL tube length L is 200 to 700 mm). Further research can be conducted about the theoretical model correlating the strength of the shock wave with the energy of the NONEL tube.

4.2 Repeatability

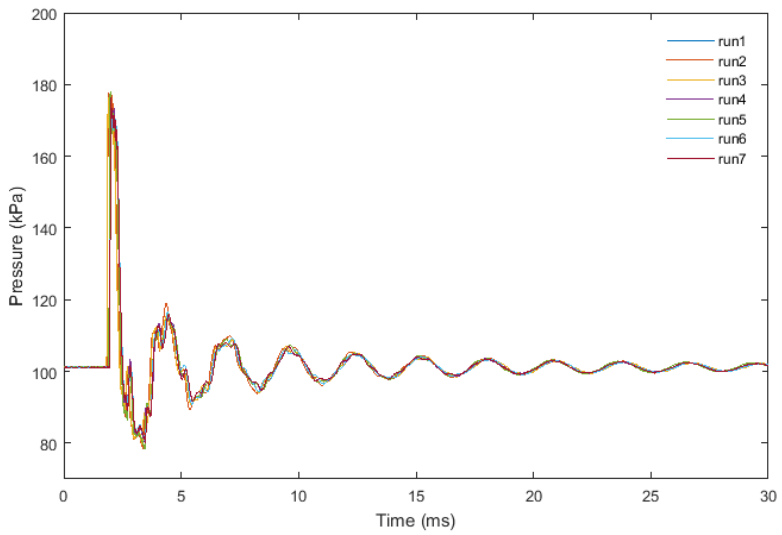

(a) The pressure history in the driven section (NONEL tube length L = 200 mm was used)

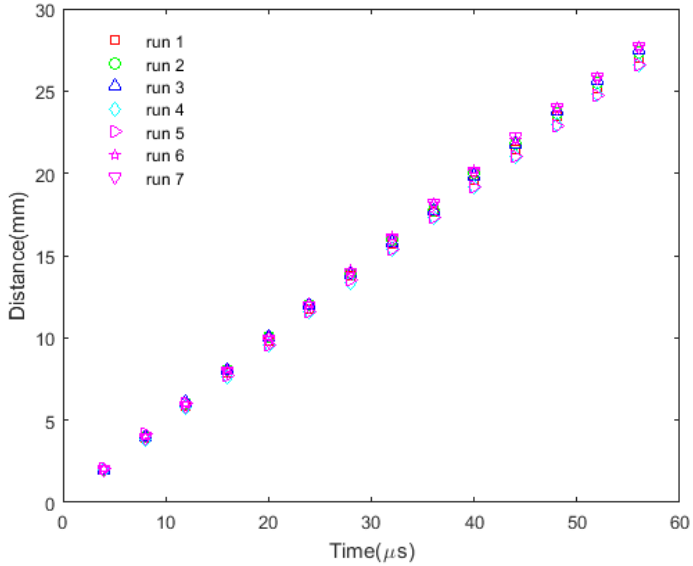

(b) The shock wave position from the open end (NONEL tube length L = 300 mm was used)

Fig. 6 Repeatability of the detonation transmission tubing driven shock tube

In different runs, there is deviation due to biases of the NONEL tube length, distribution inhomogeneity of the explosive material of the NONEL tube or other operation errors. To validate the reliability of the shock tube, the pressure measurement and flow visualization were repeated in the same experimental conditions, namely the same NONEL tube length and the same acquisition configuration including the time delay for the image capturing, exposure time and frame rate. Figure 6 (a) presents the repeatability of pressure history in the driven tube. The overpressure was 178.89 ± 2 kPa corresponding to a shock Mach number of 1.29 ± 0.01 and a repeatability of less than 2% in seven runs. Figure 6 (b) shows the instantaneous positions of the initial shock wave in shadowgraph images. The initial shock wave locations for different runs qualitatively match very well when the elapsed time of shock wave out of the open end is less than 30 μs. As the shock wave propagates further, the error is accumulated. The repeatability of shock wave location from the open end is calculated quantitatively by the equation as follows:

$$Error = abs(\frac{x_i - x_m}{x_m}) \quad (2)$$

where x_m and x_i denotes the arithmetic mean location of all the runs and the initial shock wave location of one sample run, respectively. The repeatability error of the shock wave position was found less than 3%.

4.3 The structure of flow from the open end

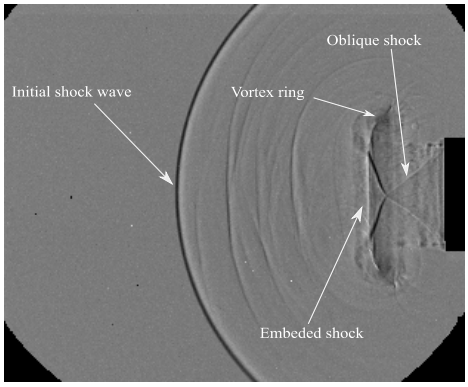

Fig. 7 Structure of the flow from the open end (L = 600 mm, Δt = 136 μs)

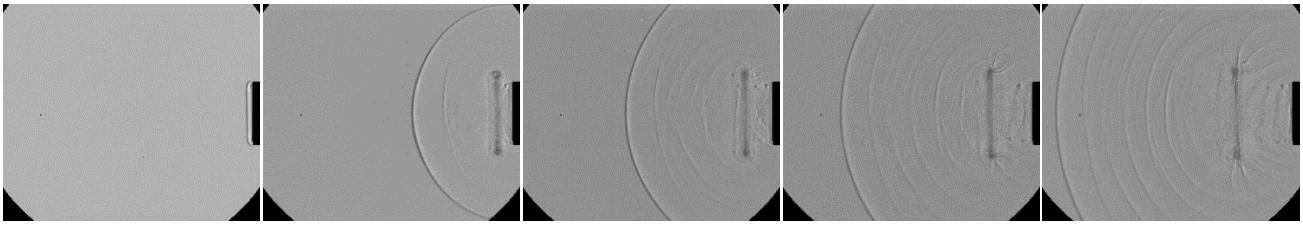

(a) Δt = 4 μs (b) Δt = 88 μs (c) Δt = 136 μs (d) Δt = 184 μs (e) Δt = 232 μs

Fig. 8 Framing shadowgraph images showing flow structure evolution from the open end, L = 300 mm.

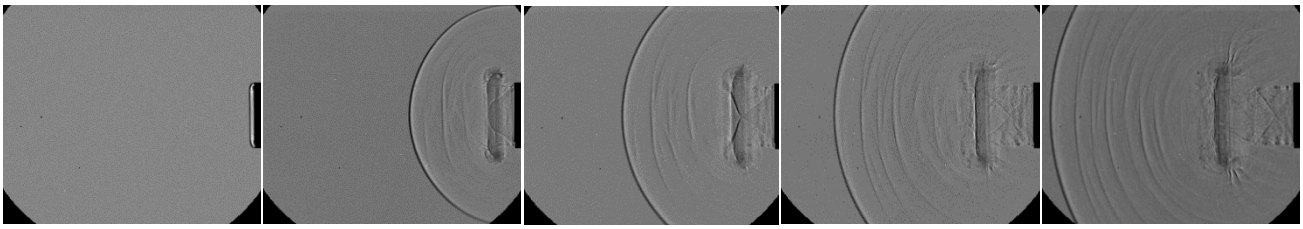

(a) Δt = 4 μs (b) Δt = 88 μs (c) Δt = 136 μs (d) Δt = 184 μs (e) Δt = 232 μs

Fig. 9 Framing shadowgraph images showing flow structure evolution from the open end, L = 600 mm.

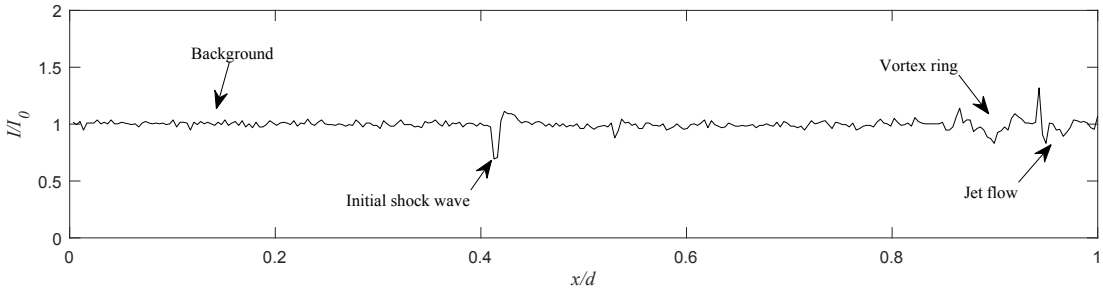

Fig. 10 Image intensity profile along the axis of symmetry of the shock tube, L= 300 mm, Δt =136 µs

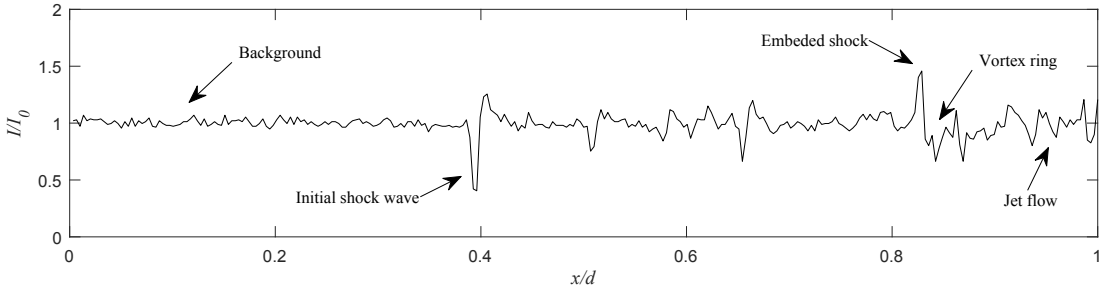

(a) Δt = 136 μs

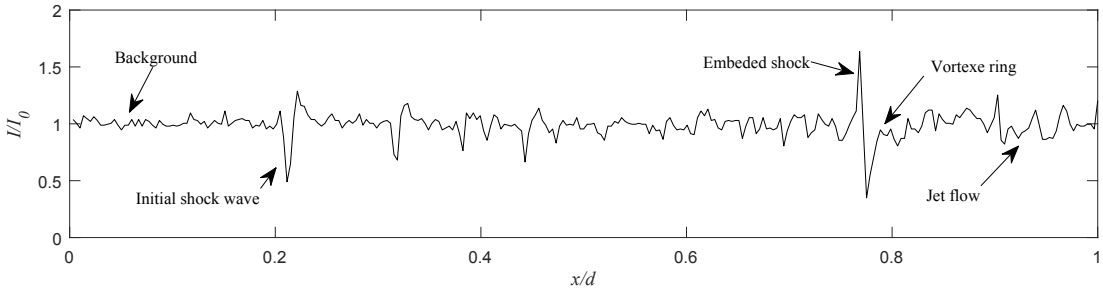

(b) Δt = 184 μs

Fig. 11 Intensity profiles along the axis of symmetry of the shock tube, L = 600 mm.

Figure 7 shows the demonstration of the primary flow structure from the shock tube open end in the case of NONEL tube length L = 600 mm and the elapsed time of the initial shock wave Δt = 136 μs. Flow structure consists of an initial shock wave, a vortex ring, an embedded shock wave and the crossed-oblique shock waves. These flow pattern corresponds well to that of conventional compressed-gas driven shock tubes [10, 31]. More detailed shadowgraph images showing the flow evolution emitting from the open end are given in Figs. 8 and 9 (NONEL tube length L = 300 and 600 mm, respectively). A planar shock wave emits from the shock tube open end (Figs. 8 (a) and 9 (a)), which validates the previous discussion in Section 2 that the hemispherical blast shock wave transforms to a plane shock wave. After emitting from the open end, the shock wave is diffracted and turns to a spherical shape as it travels. On the other hand, the air flow in the driven section behind the initial shock wave is released and forms a shear layer with external fluid. This shear layer is subsequently carried away from the edge of the detonation transmission tubing driven shock tube, rolling up to form the vortex ring. Behind the vortex ring, a jet flow with the typical oblique shock pattern is generated (Figs. 7, 8 (c) and 9 (c)). At some distances, further downstream of the open end, the vortex ring leaves from the crossed-oblique shock waves (Figs. 8 (e) and 9 (e)). It is worth noting that the increase of the incident shock Mach number Ms (NONEL tube length L increases from 300 to 600 mm) results in the generation of an embedded rearward-facing shock wave (Figs. 7 and 9). The embedded rearward-facing shock wave extends between the internal vortex cores and travels with the vortex ring.

In order to examine the evolution of the flow feature quantitatively, the intensity profiles of

shadowgraph images along the axis of symmetry of the shock tube were obtained (Figs. 10 and 11) using the in-house developed software [30]. The intensity of shadowgraph images was normalized by the brightness of the image background to subtract the unchanged magnitude from the image. The lateral axis *x/d* denotes the normalized distance from the shock tube open end. As shown in Fig. 10, the initial shock wave, the vortex ring, and the oblique shock pattern in the jet flow are detected in the intensity profile curve in the case of L = 300 mm and Δt = 136 μs. However, there is not an obvious embedded shock wave in the vortex ring in this case. By contrast, a relatively strong embedded shock wave can be found for the case of L = 600 mm, Δt = 136 μs (Figs. 11 (a)). Meanwhile, it can be seen from Figs. 10 and 11 that the intensity of the initial shock wave for the case L = 600 mm is higher than that of L = 300 mm (the higher intensity gradient implies a steeper density gradient). Comparing with Figs. 10 and 11 (a), the initial shock wave and the vortex ring in the case of NONEL tube length L = 600mm move further away from the open end than that of the L = 300 mm, which means the velocities of the initial shock wave and the vortex ring are higher in the case of larger NONEL tube length. Moreover, shocklets between the initial shock wave and the vortex ring are more apparent. The jet flow after the vortex ring becomes more complicated for the longer NONEL tube length case. Figure 11 (b) presents the intensity profile of the shadowgraph image along the axis of symmetry of the shock tube at L = 600 mm and Δt = 184 μs. By measuring the distance of the initial shock wave in different shadowgraph images, the shock velocity can be determined (Fig. 5).

5. Conclusion

A novel concept to design shock tube driven by detonation transmission tubing in a safe, repeatable, and controllable manner for laboratory scale experiments is proposed and demonstrated in this study. Specifically, a circular cross-section and open-ended shock tube with a straight driven section (inner diameter ID = 22 mm, driven section length L_d = 330 mm) is employed. The pressure histories in the driven section and the time-resolved shadowgraph images show that the induced flow structure of the detonation transmission tubing driven shock tube is similar with that of a conventional compressed-gas driven shock tube. Moreover, the shock tube driven by detonation transmission tubing has good repeatability of less than 2% with a Mach number range from 1.29 to 1.58 when the NONEL explosive mixture varies from 3.6 mg to 12.6 mg.

Compared with the conventional compressed-gas shock tubes, the shock tube driven by detonation transmission tubing is much easier to manufacture and more cost-effective. it is useful in aerodynamics research to investigate the flow including the shock wave, the vortex loop, the jet flow, and so on. In addition, it is applicable to medicine, biology and industry for various applications to replace other types of shock tubes. This study suggested that investigations such as using different nozzle contours

to improve its Mach number range, the influence of the shock tube diameter or cross-section shape and extending it into the close-ended shock tube can be performed.

Acknowledgments

The authors are grateful to Mr. Geng Qiao who helped us a lot in doing the experiment. Special thanks to Mr. Neil Owen, the electronics technician of school of engineering in the University of Glasgow for designing the signal conditioner, Mr. Alistair Macfarlane for manufacturing the shock tube and Professor Lucas for providing access to the high-speed camera.

References

[1] H. J. Davis, H. D. Curchack, S. United, and W. D. C. Harry Diamond Laboratories, *Shock tube techniques and instrumentation*. Washington, D.C.: U.S. Army Material Command, Harry Diamond Laboratories, 1969.

[2] J. N. Bradley, "Shock waves in chemistry and physics," John Wiley & Sons, Inc.; First edition, 1962.

[3] A. G. Gaydon and I. R. Hurle, *The shock tube in high-temperature chemical physics*. London: Chapman and Hall, 1963.

[4] J. H. Arakeri, D. Das, A. Krothapalli, and L. Lourenco, "Vortex ring formation at the open end of a shock tube: A particle image velocimetry study," *Physics of Fluids,* vol. 16, no. 4, pp. 1008-1019, 2004.

[5] A. C. Haselbacher, S. Balachandar, and S. W. Kieffer, "Open-Ended Shock Tube Flows: Influence of Pressure Ratio and Diaphragm Position," *AIAA Journal,* vol. 45, no. 8, pp. 1917-1929, 2007.

[6] A. Kiverin and I. Yakovenko, "On the mechanism of flow evolution in shock-tube experiments," *Physics Letters A,* vol. 382, no. 5, pp. 309-314, 2018.

[7] E. Y. Koroteeva, I. A. Znamenskaya, F. N. Glazyrin, and N. N. Sysoev, "Numerical and experimental study of shock waves emanating from an open-ended rectangular tube," *Shock Waves,* journal article vol. 26, no. 3, pp. 269-277, 2016.

[8] R. Mariani and K. Kontis, "Experimental studies on coaxial vortex loops," *Physics of Fluids,* vol. 22, no. 12, 2010.

[9] R. Mariani, M. K. Quinn, K. Kontis, and L. Marraffa, "Shock-free compressible vortex rings impinging on a stationary surface: Effects of surface angle variation," *Experimental Thermal and Fluid Science,* vol. 47, pp. 126-142, 2013.

[10] H. D. Ng, B. B. Botros, J. Chao, J. M. Yang, N. Nikiforakis, and J. H. S. Lee, "Head-on Collision of a Detonation with a Planar Shock Wave," *Shock Waves,* journal article vol. 15, no. 5, pp. 341-352, 2006.

[11] M. Thangadurai and D. Das, "Characteristics of counter-rotating vortex rings formed ahead of a compressible vortex ring," *Experiments in Fluids,* journal article vol. 49, no. 6, pp. 1247-1261, 2010.

[12] T. Ukai, H. Zare-Behtash, K. Kontis, and S. Obayashi, "Three-dimensional shock wave distortion in shock-square vortex loop interaction," *Experimental Thermal and Fluid Science,* vol. 79, pp. 85-90, 2016.

[13] H. Zare-Behtash, K. Kontis, and N. Gongora-Orozco, "Experimental investigations of compressible vortex loops," *Physics of Fluids,* vol. 20, no. 12, 2008.

[14] B. Hammer and H. Olivier, "Experimental characterization of the transonic test section flow in a Ludwieg tube," Aerospace Science and Technology, vol. 81, pp. 249-258, 2018.

[15] A. Khatta and J. Gopalan, "Hypersonic shock tunnel studies of Edney Type III and IV shock interactions," Aerospace Science and Technology, vol. 72, pp. 335-352, 2018.
[16] R. Sriram and G. Jagadeesh, "Shock tunnel experiments on control of shock induced large separation bubble using boundary layer bleed," Aerospace Science and Technology, vol. 36, pp. 87-93, 2014.
[17] E. Courtney, A. Courtney, and M. Courtney, "Shock tube design for high intensity blast waves for laboratory testing of armor and combat materiel," Defence Technology, vol. 10, no. 2, pp. 245-250, 2014.
[18] S. Downes, A. Knott, and I. Robinson, "Towards a shock tube method for the dynamic calibration of pressure sensors," *Philos Trans A Math Phys Eng Sci,* vol. 372, no. 2023, p. 20130299, 2014.
[19] E. F. Médici and G. P. Waite, "Experimental laboratory study on the formation of multiple shock waves observed during volcanic eruptions," *Geophysical Research Letters,* vol. 43, no. 1, pp. 85-92, 2016.
[20] S. R. Nanda, S. Agarwal, V. Kulkarni, and N. Sahoo, "Shock Tube as an Impulsive Application Device," *International Journal of Aerospace Engineering,* vol. 2017, pp. 1-12, 2017.
[21] Y.-L. Ning and Y.-G. Zhou, "Shock tubes and blast injury modeling," *Chinese Journal of Traumatology,* vol. 18, no. 4, pp. 187-193, 2015.
[22] D. V. Reneer, R. D. Hisel, J. M. Hoffman, R. J. Kryscio, B. T. Lusk, and J. W. Geddes, "A multi-mode shock tube for investigation of blast-induced traumatic brain injury," *J Neurotrauma,* vol. 28, no. 1, pp. 95-104, Jan 2011.
[23] A. S. Shah Ms, B. D. Stemper Phd, and F. A. Pintar Phd, "Development and characterization of an open-ended shock tube for the study of blast mtbi,", *Biomed Sci Instrum,* vol. 48, pp. 393-400, 2012.
[24] M. S. Downey, T. J. Cloete, and A. D. B. Yates, "A rapid opening sleeve valve for a diaphragmless shock tube," *Shock Waves,* vol. 21, no. 4, pp. 315-319, 2011.
[25] D. C. Taylor, "The characterization and feasibility of a low-duty-cycle diaphragmless shock tube,", 2012.
[26] S. Janardhanraj and G. Jagadeesh, "Development of a novel miniature detonation-driven shock tube assembly that uses in situ generated oxyhydrogen mixture," *Rev Sci Instrum,* vol. 87, no. 8, p. 085114, 2016.
[27] Y. Kai, W. Garen, T. Schlegel, and U. Teubner, "A novel shock tube with a laser–plasma driver " *Laser and Particle Beams,* vol. 35, no. 04, pp. 610-618, 2017.
[28] H. Zare-Behtash, N. Gongora-Orozco, K. Kontis, and G. Jagadeesh, "Study of Detonation Interactions Inside a Two-Dimensional Ejector Using Detonation Transmission Tubing," *Journal of Propulsion and Power,* vol. 26, no. 4, pp. 878-882, 2010.
[29] I. O. Samuelraj, G. Jagadeesh, and K. Kontis, "Micro-blast waves using detonation transmission tubing," *Shock Waves,* vol. 23, no. 4, pp. 307-316, 2012.

[30] G. Li, M. BurakAgir, K. Kontis, T. Ukai, and S. Rengarajan, "Image Processing Techniques for Shock Wave Detection and Tracking in High Speed Schlieren and Shadowgraph Systems," Journal of Physics: Conference Series, vol. 1215, 2019.

[31] H. Zare-Behtash, "Experimental studies on compressible vortical flows, phenomena and interactions," Doctoral dissertation, Engineering and Physical Sciences, University of Manchester, 2009.